Visible photoluminescence from nanocrystallite Ge embedded in a glassy SiO_2 matrix: Evidence in support of the quantum-confinement mechanism

Yoshihito Maeda
Hitachi Research Laboratory, Hitachi, Ltd., 7-1-1 Ohmika-cho, Hitachi, Ibaraki 319-12, Japan
(Received 1 August 1994)

Nanocrystallite Ge (nc-Ge) embedded in a glassy SiO_2 matrix is fabricated and examined by x-ray photoelectron spectrometry, Raman spectrometry, and high-resolution transmission-electron microscopy. The precipitation and growth of nc-Ge are found to be related to a thermodynamical reduction of GeO_2, the diffusion of Si atoms from the Si substrate into the glassy matrix, and an aggregation of small-sized nc-Ge. The size inhomogeneity can be precisely controlled by a double annealing, and the average size can be changed in the range of 2–6 nm. Broadband photoluminescence (PL) spectra are observed in the visible wavelength range at room temperature, and they exhibit pronounced blueshifts of the peak energies and broadening of the PL spectra, which can be correlated to the change in the size. The PL excitation spectra show a Stokes energy smaller than 0.1 eV and dependence on the measurement energy. The visible PL also shows a strong correlation to the presence and actual condition (i.e., size) of nc-Ge. Possible origins of the visible PL such as a quantum-confinement model in quantum dots, the presence of luminescent centers (Ge:E') in silica glass, or a structural transition of nc-Ge are discussed. The present experimental data are concluded to be more consistent with a quantum-confinement model than with the other models.

I. INTRODUCTION

Recently, attempts have been made to fabricate quantum-size structures based on silicon or germanium, in which usually indirect optical transition takes place between the band gap so that the radiative efficiency is limited to a very small value. Canham[1] has reported that intense visible photoluminescence (PL) could be observed at room temperature from anodically etched silicon, i.e., porous silicon (porous Si), and the microstructure of porous Si was of a quantum wire or train of quantum dots (QD's). A number of researchers have already proposed models for the mechanism of visible PL related to quantum confinement in nanocrystallite Si incorporated in porous Si or of another origin.[2]

In comparison with electronic properties of Si, Ge has a larger dielectric constant and smaller effective masses for electrons and holes, and the energy difference ($\Delta E = 0.12$ eV) between the indirect gap ($E_g = 0.66$ eV at 300 K, $\Gamma'_{25} - L_1$) and the direct gap ($E_0 = 0.8$ eV: $\Gamma'_{25} - \Gamma'_2$) is smaller. The effective Bohr radius a_B for Wannier excitons in Ge is calculated to be about 24 nm. These electronic conditions lead to an expectation that it is much easier to change the electronic structure around the band gap of Ge.

Based on this viewpoint, Maeda *et al.*[3] have fabricated a glassy SiO_2 matrix that contained a very large amount of quantum-size nanocrystallite Ge (nc-Ge) with an average size of 6–8 nm. They reported an intense yellowish orange photoluminescence around 2.2 eV at room temperature. Kanemitsu *et al.*[4] measured radiative decay for nc-Ge of average size of 4.2–14.4 nm. They observed a single-exponential decay with almost the same decay time of 850–900 ps for all sizes. They discussed instability of the diamond structure in very small crystallites and suggested the possibility of a phase change from the diamond to tetragonal structures as the origin of PL, based on electron microscopic observations. Venkatasubramanian *et al.*[5] have also observed PL near 1.9 eV from a nanometer-sized planar Ge structure fabricated by plasma-assisted etching using a CF_4/O_2 gas mixture. Paine and co-workers[6,7] have observed strong visible PL from nc-Ge that was made by a completely different method than used in other studies; they utilized a chemical reduction of an oxide alloy of $Si_{1-x}Ge_xO_2$ formed by high-pressure oxidation. Prior to these visible PL observation studies, Fujii, Hayashi, and Yamamoto[8] and Hayashi *et al.*[9] reported a very clear blueshift of the optical absorption edge for nc-Ge embedded in a glassy SiO_2 matrix as the average crystallite size decreased. But such clear size dependence of the PL peak energy has not been observed yet. Its absence has been considered to be due to a very broad spectrum coming from size inhomogeneity or the inherent electronic band structure in Ge or due to a large difference between the absorption and radiation procedures.

Much attention has been paid to this visible PL from indirect semiconductor QD's. Quantum-confinement theory leads to an expectation that this visible PL is made possible by band-gap widening due to quantized levels and significant modulation of the usual electronic band structure in the band gaps, such as the change from an indirect gap to a direct gap, so that radiative efficiency may be enhanced at room temperature. To study details of the visible PL, we have to characterize the size inhomogeneity and find a way to control the average size and distribution as much as possible.

In this paper, details of precipitation of nc-Ge from a

 ©1995 The American Physical Society

supersaturated solid solution during annealing are examined by high-resolution transmission-electron microscopy (HR-TEM) and other characterization methods. Then careful control of the average size is attempted by a double-isothermal annealing procedure, the principle of which comes from crystal nucleation and growth theory. The properties of the visible PL from nc-Ge with well-controlled size are examined to establish a correlation to the results predicted by three-dimensional confinement theory. Finally, other possible mechanisms on the origin of visible PL are discussed.

II. EXPERIMENTAL DETAILS

A. Sample preparation

Glassy-matrix films including nonstoichiometric Si and Ge oxides were deposited onto Si ⟨001⟩ substrates with about 3–5-nm-thick native oxide by a radio-frequency (rf) magnetron-sputtering deposition method. The deposited films were 0.7–2.5 μm thick. The rf power of 1.5 kW was applied between the target and substrate holder, and the argon partial pressure was held at 3×10^{-3} Torr during deposition by using a mass-flow controller. The substrate holder was kept at about 30 °C by circulating water. The chamber was evacuated with a cryovacuum pump. The attainable vacuum rate was less than 5×10^{-5} Pa. The sputtering target of 99.99% pure SiO_2 (100 mm diameter) and some Ge chips ($5\times5\times1$ mm^3) of 99.9999–99.999 99 % purity were employed. These chips were set on the target in a circle. The film thickness was measured by scanning electron microscopy (SEM). The chemical composition of the as-deposited sample was analyzed by inductive-plasma optical-emission spectrometry. The typical amount of elemental Ge was 42–46 mol % in the SiO_2 matrix and no impurities were detected, except of Fe of less than 1 ppm.

After deposition the sample was isothermally annealed to get large amounts of nc-Ge in the matrix. The isothermal annealing was carried out in an electrical furnace or on a hot stage in an argon atmosphere at 300–800 °C. The temperature fluctuation was controlled with 1 °C. The temperature rising rate to reach the annealing temperature was 60–90 °C/min.

B. Sample characterization

Chemical bonding in the matrix was analyzed by x-ray photoelectron spectrometry (XPS). The Mg $K\alpha$ radiation ($h\nu=1303$ eV) was used for excitation and the sample film was etched by Ar sputtering to examine the depth profile. To avoid charging effects in XPS measurements, an energy correction of the spectrum was carried out using the energy of photoelectrons from the Ar $2p_{3/2}$ level ($h\nu=242.0$ eV).

The precipitation of nc-Ge in the cross-sectional image was observed with HR-TEM to examine crystallinity and statistical size distribution. To thin the sample ($t\leq5$ nm), it was mechanically polished and then etched by Ar sputtering. With these sample-preparation techniques, nc-Ge embedded in the glassy matrix could not be damaged, but whether there was an unavoidable thermal effect during etching (carried out below 200 °C) on the precipitation was uncertain. The cross-sectional structure was observed by SEM. The sample was cleaved in liquid nitrogen to get a smooth cross section and then the surface was coated with a very thin carbon film to prevent charging effects.

C. Statistics

The statistics, i.e., size and number, of crystallites were obtained directly from cross-sectional HR-TEM images taken of a 57.50×43.25 nm^2 area. The observed volume was calculated as approximately $7.4-14.8\times10^4$ nm^3, assuming that the thickness was 5 nm. To minimize statistical error of the population, by using as many images as possible taken in different places, a large total number of nc-Ge should be counted. The size was defined by Brown size, which corresponds to the longest dimension of the crystallite. This definition allowed us to regard crystallites with different crystal habits and morphologies as spherical crystallites. This assumption has been employed in various crystallite systems and it provides size distributions, which are consistent with physical models for crystal nucleation and the growth procedure in glassy matrices, without any inherent directions for the crystal growth.

D. Spectroscopic measurements

Raman spectra of samples were excited with the 780-nm laser line from a tunable titanium-sapphire laser (Ti-sapphire laser) pumped by a 4-W cw multimode Ar-ion laser. The excitation power was usually 10 mW/cm^2 during measurements. The spectra were detected with a double monochromator (focusing length =1 m), a GaAs(Cs) photomultiplier, and a photon-counter unit. The measurement of the sample on the silicon substrate was carried out at room temperature. The incident laser beam was focused onto a 0.1-cm-diam spot. PL measurements were conducted using a cw Ar-ion laser line at 488-nm or a cw He-Cd laser line at 325 nm at room temperature in air. The power density of the excitation beam was 1–10 mW/cm^2. The PL was detected with the same system as used in the Raman spectral measurements. The PL spectra over the visible region were corrected by the transmittance of the monochromator and the quantum efficiency of the photomultiplier. The photoluminescence excitation (PLE) spectra were measured with a fluorescence spectrophotometer using a Xe arc lamp (250 W) and a double monochromator.

III. RESULTS

A. Precipitation of nanocrystallite Ge

Figures 1(a) and 1(b) show respective SEM images for the cross sections of as-deposited and annealed samples that were formed on Si substrates. In Fig. 1(a) the as-deposited sample shows particle growth near the Si substrate and columnar growth with many corrugations, asperities, and crevices in the particle-growing layer. In the sample annealed at 800 °C for 30 min shown in Fig. 1(b),

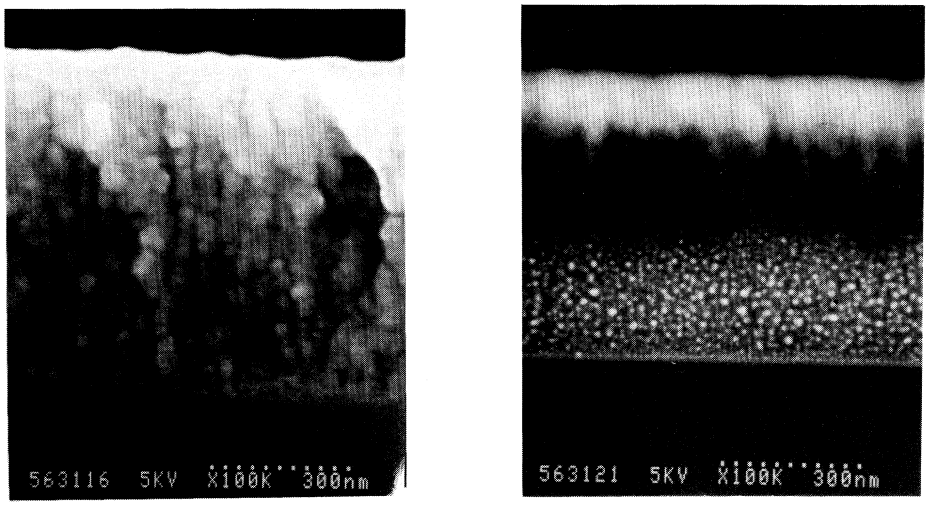

FIG. 1. Cross-sectional SEM images for (a) the as-deposited sample and (b) the annealed sample (800 °C, 30 min).

a large number of nc-Ge (bright points) are observed to precipitate densely in a layer close to the Si substrate. In such a precipitation layer the spatial distribution of nanocrystallites is uniform. This shows that there is no dominant place for crystal nucleation; namely, homogeneous nucleation takes place in the precipitation layer.

Figure 2 shows Raman spectra of optical phonons (TO-like mode: Γ'_{25}) near 300 cm^{-1} coming from nc-Ge embedded in the glassy SiO_2 matrix and a very strong scattering line from the Si substrate. These spectra were excited by the 1.6-eV (780 nm) line of a titanium-sapphire laser to prevent strong PL during measurements. The

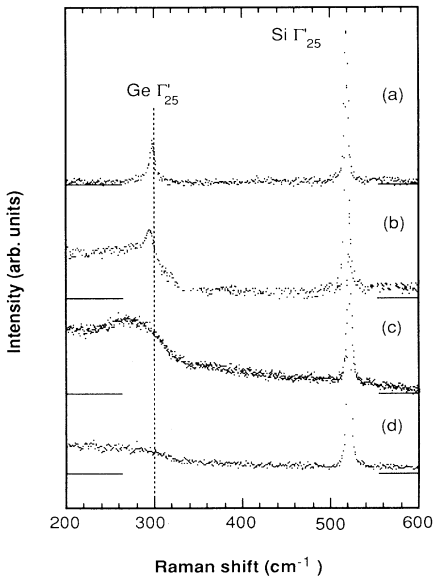

FIG. 2. Raman spectra for the samples annealed at (a) 800 °C, (b) 600 °C, and (c) 300 °C. The Raman spectrum for (d) was obtained in the as-deposited sample. The spectra were excited by a 780-nm titanium-sapphire laser of 10 mW. The narrow band line at 520 cm^{-1} comes from the Si substrate.

Raman spectrum of the as-deposited sample does not show a clear peak associated with the TO-like mode of diamond Ge. As the annealing temperature was raised above 300 °C, the broad bump that appears near 300 cm^{-1} narrowed and at the same time its peak position shifted toward a higher wave number. The quantum-confinement theory of phonons shows that the broadening and peak shift correspond to an increase in the average size of nc-Ge. Fujii, Hayashi, and Yamamoto[8] used this theory to relate peak breadth (fill width at half maximum) to the average nanocrystallite size. For the sample annealed below 300 °C, there is a bump but no peak near 300 cm^{-1}, in obvious difference to the spectrum of the as-deposited sample. This may come about from differences in the amount of incorporated amorphous-Ge (*a*-Ge) and the oxide in the glassy SiO_2 network, because this broad bump can be separated into peaks for *a*-Ge and the Ge oxide. The presence of nc-Ge in the glassy matrix annealed at 300 °C was examined by HR-TEM. The HR-TEM observation indicates that its local structure differs from that of the sample annealed at high temperature. In Fig. 3, we can see very small nc-Ge. The lattice fringes and the interfaces cannot be clearly resolved in the dark areas of the HR-TEM image. In the high-resolution images of this sample, there are many dark areas in the matrix, in which almost all nanocrystallites precipitate. These inhomogeneous dark areas may be due to the inhomogeneity of Ge concentration in the glassy matrix or due to crystallites that are not oriented in a way that allows lattice fringes to be observed. This change in the contrast has also been observed in a composite containing elements with different atomic numbers and masses from the present sample. In fact, there is no contrast inhomogeneity in the image of the as-deposited sample. This inhomogeneity increase in the matrix may be related to thermodynamical reduction of the Ge oxides, which are present initially in the glassy matrix.

In other samples prepared by the same sputtering-deposition method as used in this paper, the absence of nc-Ge was reported in the sample annealed below 600 °C,

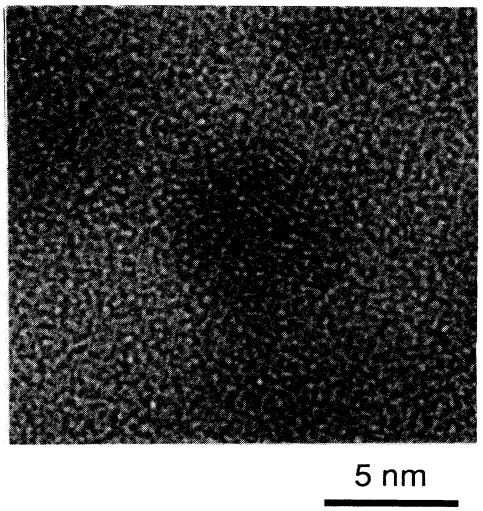

FIG. 3. HR-TEM image of 2–3-nm-sized nc-Ge with diffuse lattice fringes. The annealing was carried out at 300 °C for 30 min.

even in the HR-TEM dark-field images.[9] This difference between the observations may be related to a difference in the initial chemical component and the presence of Ge oxides.

B. Thermodynamical reactions

Figure 4 shows x-ray photoelectron spectra in the binding energy range of Ge $3d_{5/2}$. In the spectrum for the as-deposited sample two pronounced peaks appear. The peak at 29.3 eV originates from Ge $3d_{5/2}$ electrons and that at 32.6 eV corresponds to GeO_2 with a chemical shift of 3.3 eV from elemental Ge. According to the phase diagrams, a small amount of elemental Ge (less than 1 at. %) can dissolve in quartz SiO_2, while a large amount of GeO_2 (~20 mol %) can dissolve in quartz SiO_2. In the sample, large amounts of excess Ge and oxides are incorporated into the glassy SiO_2 matrix. No phase separation is observed in the HR-TEM image of the as-deposited matrix. Therefore, this glassy SiO_2 matrix is a supersaturated solid solution containing a large amount of excess Ge. When the sample is annealed at temperatures from 300 to 800 °C for 30 min, both an increase of Ge corresponding to precipitation of nc-Ge in the matrix and a decrease in the amount of GeO_2 occur simultaneously. With increased annealing temperature, the amount of GeO_2 decreases significantly. Since the increase in Ge must be related to a decrease in GeO_2, GeO_2 may be reduced in the matrix by some thermodynamical reactions during annealing. Some thermodynamically possible reactions can describe formation of elemental Ge in SiO_2. The simplest reaction is a direct decomposition of GeO_2 given by $GeO_2=Ge+O_2$. Using thermodynamical data[10] we can calculate the Gibbs energy at thermodynamical equilibrium, $\Delta G=\Delta G_f+RT\ln K$, where R and K are the gas constant and the equilibrium constant at temperature T, respectively. At 1000 K, $\Delta G=0$ and $\Delta G_f=-387.1$ kJ/mol; therefore we can calculate the

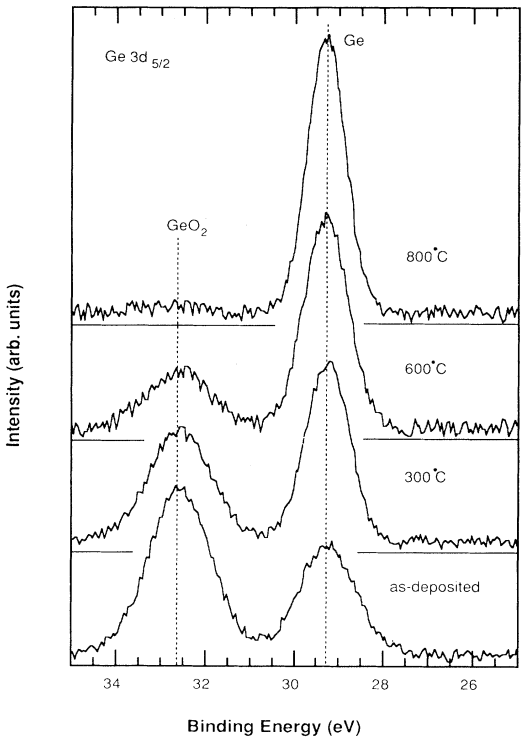

FIG. 4. Annealing temperature dependence of x-ray photoelectron spectra in the binding-energy range of Ge $3d_{5/2}$. The binding energy was calibrated with the Ar $2p_{3/2}$ binding energy.

equilibrium partial pressure of oxygen gas as $P_{O_2}=6.1\times10^{-21}$ atm. This P_{O_2} is much larger than that of SiO_2 (7.16×10^{-39} atm) at the same temperature, but we cannot expect such direct decomposition at 1 atm and need some reductants for reduction of GeO_2 in the matrix.

As one candidate reductant, elemental Si can be considered. The displacement reaction between GeO_2 (*tetragonal*), Si, SiO_2 (*trigonal or hexagonal*), and Ge can be considered to take place as written by

$$GeO_2+Si=SiO_2+Ge\ .$$

From the Gibbs energy at thermodynamical equilibrium of the reaction, we can tell whether this reaction can proceed spontaneously at the temperature or not. The Gibbs energies of formation are $\Delta G_f=-462.492$ and -368.598 kJ/mol for pure GeO_2 and $\Delta G_f=-801.367$ and -712.844 kJ/mol for pure SiO_2 at $T=600$ K (327 °C) and 1100 K (827 °C), respectively.[11] The change in the Gibbs energy of the displacement reaction is $\Delta G_f=-338.875$ and -344.246 kJ/mol at $T=600$ and 1100 K, respectively. This thermodynamical consideration shows that elemental Ge is very stable in a SiO_2 network and this displacement reaction can proceed spontaneously at the interface between GeO_2 and Si at ~300 °C , and this reaction requires interdiffusion of the same amount of elemental Si to that of produced Ge. Originally, the SiO_2 matrix includes an excess amount of elemental Si incorporated in it due to nonstoichiometry

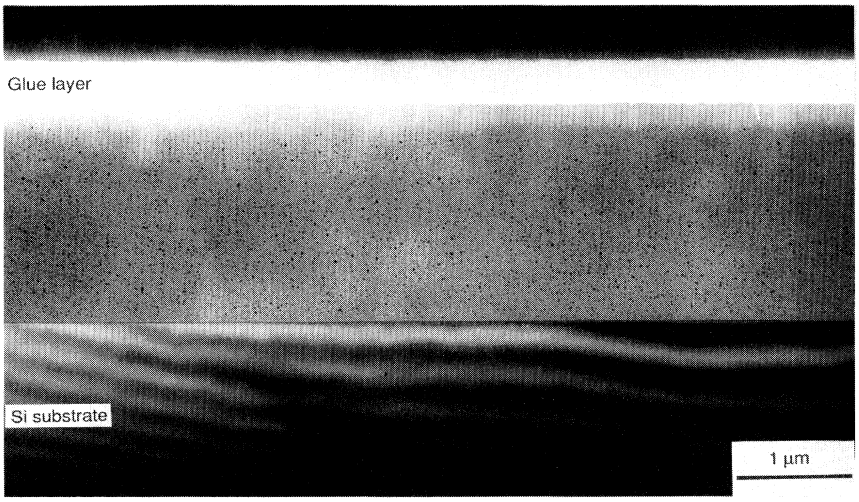

FIG. 5. Cross section of the matrix exhibiting a large number of nc-Ge in a precipitation layer.

of the matrix (lack of oxygen). The XPS in Fig. 2 reveals that almost all GeO_2 present in the matrix can be reduced during annealing at 800 °C for 30 min, while such large amounts of GeO_2 cannot be reduced only by originally incorporated excess Si atoms. The largest source of Si atoms is the Si substrate on which the matrix film is deposited. In the SiO_2 matrix, Paine *et al.*[6] have reported that Si atoms diffused from the substrate to the glassy oxide alloy of $Si_{1-x}Ge_xO_2$ formed by high-pressure oxidation and the reduction took place.

C. Diffusion of Si atoms in the SiO_2 matrix

As shown in the SEM image of Fig. 1, nc-Ge precipitates only in the layer close to the Si substrate (precipitation layer), in which we can see a large number of nc-Ge. There is also a clear boundary in the HR-TEM image of Fig. 5 of the sample annealed at 800 °C for 4 h. In comparison with the precipitation layer in Fig. 1, the layer thickness in Fig. 5 increases significantly.

Figure 6 shows thickness X_b of the precipitation layer of nc-Ge measured from the Si substrate as a function of annealing time at 800 °C. The time-dependent thickness can be fitted by $X_b = 5.36t^{1/2}$. The diffusion length X is approximately given by $X \sim \sqrt{\pi Dt}$, where D is a diffusion constant of atoms. Assuming that this precipitation layer is related to the diffusion length of Si atoms from the substrate and that the displacement reaction for formation of Ge and SiO_2 can proceed very rapidly, we consider that this layer thickness X_b agrees approximately with the diffusion length of Si atoms from the substrate, therefore, $X_b \approx X_{Si} \sim \sqrt{\pi D_{Si} t}$. From the results in Fig. 4, the diffusion constant D_{Si} in the glassy SiO_2 matrix can be estimated as 2.73×10^{-13} cm^2/s. Paine, Caragianis, and Shigesato have estimated that the diffusion constant of Si atoms in the glassy SiO_2 matrix was on the order of 10^{-13} cm^2/s, for a large number of voids in the matrix, because Si cannot diffuse in the matrix without any voids. But in fact, only the matrix annealed at 800 °C has a large number of voids (or rather proves) with 15–30 nm diameter as shown in the cross-sectional SEM image of Fig. 7. These pores may originate from a big difference in the densities between Ge, GeO_2, and SiO_2. The good agreement for the diffusion constant shows that the precipitation layer might be dominated mainly by diffusion of Si atoms from the Si substrate; if GeO_2 can obtain Si at the reaction interface (around oxygen atoms in the network), the displacement reaction can proceed rapidly because of the very large driving force.

Also in the sample deposited on the quartz substrate, after annealing visible PL could be observed and the PL spectrum was almost the same as that measured in the sample on a Si substrate, except for a large difference in the PL intensity due to the difference in amounts of nc-Ge. This shows that some parts of nc-Ge can form directly from excess elemental Ge and from elemental Ge from GeO_2 reduced by excess elemental Si initially present in the SiO_2 matrix.

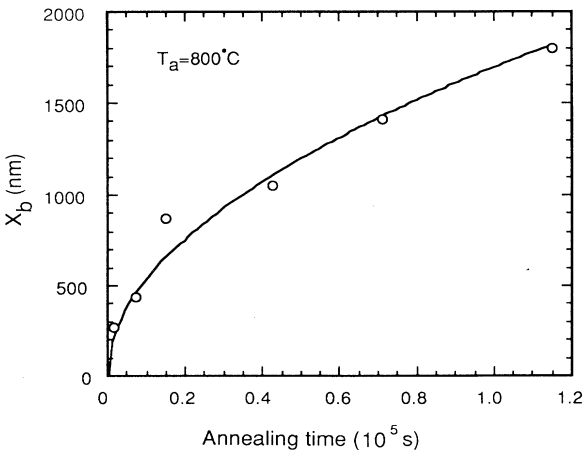

FIG. 6. Thickness of the precipitation layer X_b as a function of the annealing time.

FIG. 7. SEM image of the cross-sectional structure of the sample exhibiting a large number of pores. The surface was coated with a thin Pt film.

D. Crystallite morphology

Figure 8 shows well-grown nc-Ge with very clear interfaces and lattice fringes in the matrix of the sample annealed at 800 °C. In this image, there is no broad contrast around nc-Ge as seen in Fig. 3. The nc-Ge of Fig. 8 shows typical crystal habits of a diamond structure; this image is very close to one projection of a cuboctahedron, which consists of eight {111} planes and six {100} planes, from the ⟨100⟩ direction. Wolff and Gualtieri[12] have reported that Ge particles prepared from $GeCl_4$ could be observed to be polyhedrons with {111}, {100}, {311}, {110}, and {310} planes that could be determined by thermodynamical equilibrium (surface-energy minimum).

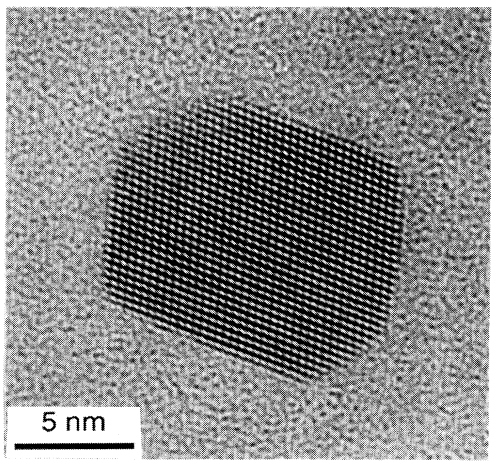

FIG. 8. HR-TEM image of well-grown nc-Ge with the actual size of 15 nm.

Figures 9(a)–9(d) show crystallite morphologies corresponding to sizes. Figure 9(a) has some nc-Ge, about 3 nm in diameter, which show no clear crystal habits and are almost spheres. In Figs. 9(b)–9(d), their crystallites (6–13 nm diam) show clear crystal habits of {111} and {100} planes. The lattice spacing obtained from the {111} plane agrees with the 3.27 Å of the {111} plane of diamond structure. The crystallite morphology can be assigned as a Wulff's polyhedron[13] (cuboctahedron) and nc-Ge has good crystallinity of diamond structure for sizes above ~5 nm. For smaller sizes (≤3 nm), even in the HR-TEM observation, we cannot get distinct nanocrystallite images that can be assigned well. For the small sizes, most nanocrystallites cannot be assigned as one plane (projection) of the diamond structure. This fact gives two possible interpretations. One is related to a lack of resolution of HR-TEM observations. The other is concerned with lattice instability, which can be predicted to take place in very small crystallites, and a phase transition from the diamond structure to something else (including an amorphous phase). Some observations on this structural change have already been reported in Si and Ge ultrafine particles prepared by evaporation in gas.[14,15] This phase transition probably changes the physical situation related to the electronic band structure.

E. Size growth

Semiconductor-doped glasses with supersaturation have been annealed isothermally to control the size of doped-semiconductor microcrystallites. In this case, annealing temperature and time are dominant factors for controlling the size. Ekimov and Onushchenko[16] and Lifshitz and Slyozov[17] have proposed models for the diffusion decomposition of a supersaturated solid solution

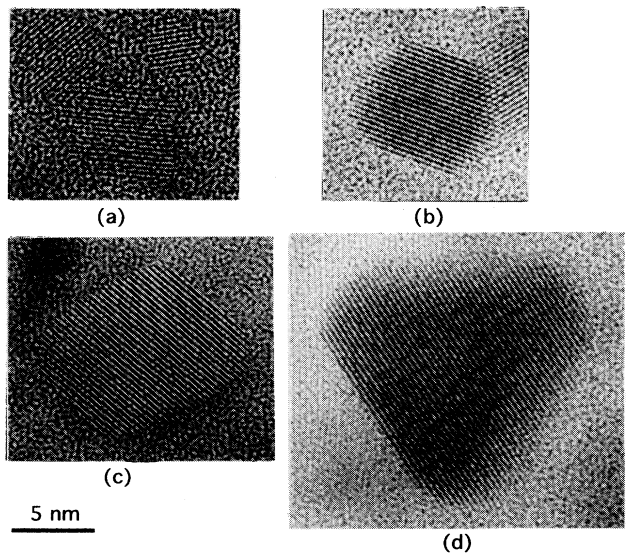

FIG. 9. Size dependence of crystallite morphologies.

in the later stage of crystalline growth and deduced the increase in the average size $\langle R \rangle$ as a function of time,

$$\langle R \rangle = (4\alpha Dt/9)^{1/3} , \quad (1)$$

where D is the diffusion coefficient and α is a coefficient related to the interphase surface tension. Hayashi *et al.*[9] prepared nc-Ge directly in glassy SiO_2 by heating the substrate at 400 °C during sputtering deposition, and reported that the increase of the average size of nc-Ge obeys the $t^{1/3}$ power law. However, in this paper, we observe that the average size of nc-Ge does not exhibit such a simple $t^{1/3}$ power-law behavior. This is because the average size might be determined not only by local diffusion of Ge initially contained in the matrix, but also by Ge produced by reduction of GeO_2 using excess Si atoms and those diffusing from the substrate. The elemental Ge initially contained in the matrix as shown in Fig. 3 can provide nuclei that grow to crystallites, if the size is sufficiently larger than the critical size. In a supersaturated solid solution, the supersaturation parameter σ is large and the driving force for the homogeneous nucleation given by $\Delta\mu = kT\ln(1+\sigma)$, is very large, where k is the Boltzmann constant, $\sigma = (C - C_{eq})/C_{eq}$, and C and C_{eq} are actual and equilibrium concentrations, respectively. The critical size can be estimated from Wulff's theorem.[13] If the polyhedron consists of only $\{111\}$ planes, the critical size $h_c^*\{hkl\}$ defined by the vertical distance between the center point of the polyhedron and the center of the $\{hkl\}$ plane and Gibbs formation energy of the critical-sized crystallite ΔG^* are given by

$$h_c^*\{hkl\} = 2v_c\gamma\{hkl\}/\Delta\mu , \quad (2a)$$

$$\Delta G^*\{hkl\} = 4\omega\gamma\{hkl\}^3 v_c^2/3\Delta\mu^2 , \quad (2b)$$

where v_c is atomic volume (Ge: $v_c = 2.27\times10^{-23}$ cm^3), $\gamma\{hkl\}$ is the surface energy density of the $\{hkl\}$ plane given by $\gamma\{hkl\} = \sqrt{3}\varphi/2a^2$ (φ: bonding energy of the first neighbor atoms; a: lattice constant), and ω is a topological constant (diamond: $\omega = 12\sqrt{3}$). In diamond-structure nanocrystalline Ge $\{111\}$ is the dominant plane; using Eqs. (2a) and (2b), $\varphi = 159$ kJ/mol, $\gamma\{111\} = 714$ erg/cm^2, and $\Delta\mu = 1.53\times10^{-13}$ erg ($\sigma = 40$) at 300 K, we obtain $h_c^*\{111\} = 10$ Å and $\Delta G^*\{111\} = 3.35$ kJ/mol. This calculated critical radius is almost the same as the observed smallest radius of nc-Ge in the HR-TEM images. This shows that under supersaturation even with a low temperature of 300 °C, nucleation can proceed easily.

In the HR-TEM observations, a peculiar growth process of nc-Ge was often observed in samples annealed at high temperature ($\geq$ 700 °C). Figures 10(a) and 10(b) show two examples, in which nanocrystallite grows from several small nc-Ge by an aggregation process. In Fig. 4(a) several nc-Ge come into contact with each other and the lattice planes are adjusted at the interface. This growth mechanism is an aggregation process of small-size nc-Ge. Above 700 °C, this kind of aggregation takes place frequently, so that the average size increases rapidly. If the aggregation rate is proportional to surface curvature of the surface of nc-Ge, the increase of the average size is proportional to the $t^{1/2}$ power law.

F. Size control

From the HR-TEM observation results of nc-Ge precipitated at several annealing temperatures, we look at a method to control the average size. Classical crystal nucleation and growth theory indicate that the temperature for homogeneous nucleation under a super-cooling condition is much lower than the temperature at which the crystalline growth rate is maximum, and that the number of nc-Ge in a unit volume and their average size depend on the nucleation frequency and growth rate, respectively. Potter and Simmons[18] have attempted to minimize size inhomogeneity in CdS glass by a double-heat-treatment procedure in which they could distinguish between crystal nucleation and growth steps.

Figure 11 shows the HR-TEM image of very small nc-Ge that is close to the critical size. The sample was annealed at 300 °C for a comparatively long time, 5 h. There are large amounts of nc-Ge densely precipitating in the glassy matrix. Their average diameter is about 2 nm. At 300 °C, when the sample was annealed isothermally the size does not increase, but the number of nc-Ge in unit area increases as the annealing time increases. The average nucleation rate $I = 4.4\times10^{14}$ cm^{-3}s^{-1} can be obtained. This shows that near this temperature $T_n \sim 300$ °C, the nucleation rate can be enhanced, and this temperature is a characteristic temperature for nucleation. In a double-isothermal annealing procedure, the sample is annealed near $T_n \sim 300$ °C, and then heated to $T_g \geq 600$ °C, at which both Si and Ge can diffuse sufficiently in the glassy matrix. The first and second an-

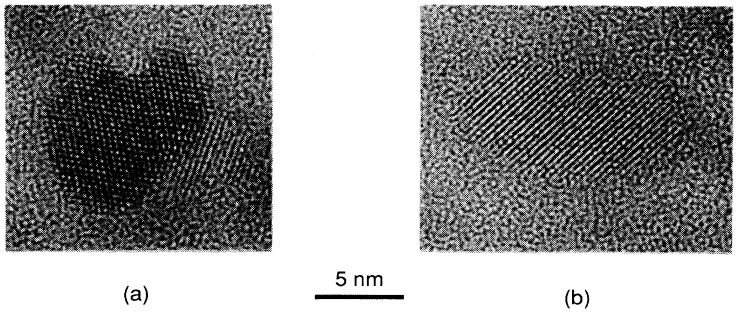

FIG. 10. HR-TEM images of nc-Ge in an aggregation process during annealing.

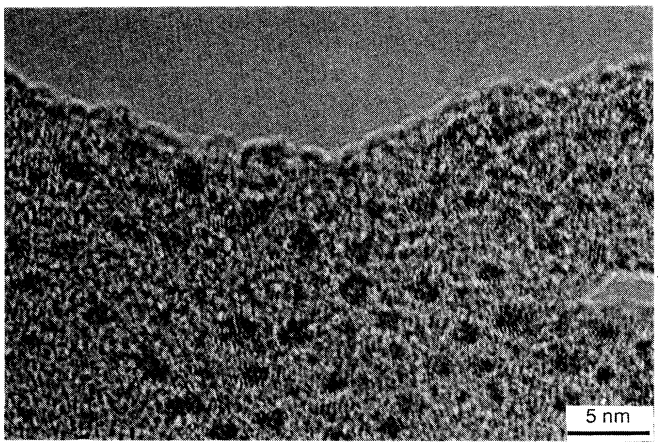

FIG. 11. HR-TEM image of very small nc-Ge close to the critical size for nucleation.

nealing procedures allow us to control the number of nuclei and growth rate, respectively. The double-isothermal annealing procedures are carried out at 300 and 600 °C for 30 min each.

Figure 12 shows the size distribution measured in the sample annealed by the double-isothermal annealing procedures. The best fitting of measured size distribution cannot be carried out by a function proposed by Lifshitz-Slyozov,[17] but by a logarithmic normal distribution function $F(d)$ given by

$$F(d)=\frac{N}{\log_{10}\sigma\sqrt{2\pi}}\exp\left[-\frac{(\log_{10}d-\log_{10}d_g)^2}{2(\log_{10}\sigma)^2}\right], \quad (3)$$

where N is the total number of counted nc-Ge,

$$\log_{10}d_g=\frac{\Sigma(n\log_{10}d)}{n}, \quad (4a)$$

$$\log_{10}\sigma=\left[\frac{\Sigma[n(\log_{10}d-\log_{10}d_g)^2]}{N}\right]^{1/2}. \quad (4b)$$

This function can be applied to an explanation of size inhomogeneity present in many kinds of nanocrystallites. In the fitting of Fig. 12(a) the average size $d_g=2.1$ nm and the size deviation $\sigma=1.28$ nm can be obtained. After this the sample was annealed at 600 °C for 30 min and the size distribution as shown in Fig. 12(b) is obtained. The average size increases to $d_g=3.1$ nm and the size deviation also increases to 1.33 nm. Then the sample was annealed again at 600 °C for 30 min. The average size increases to $d_g=4.4$ nm and the size deviation also increases to 1.49 nm in Fig. 12(c). At 600 °C large numbers of nc-Ge more than 5 nm in diameter can be formed. These results show that we can control the average size from 2.1 to 4.4 nm and the size deviation from 1.28 to 1.49 nm more precisely by the double-annealing procedure carried out at two characteristic temperatures ($T_n\sim300$ °C and $T_g\geq600$ °C) for nucleation and growth, rather than by the usual annealing procedure at one temperature.

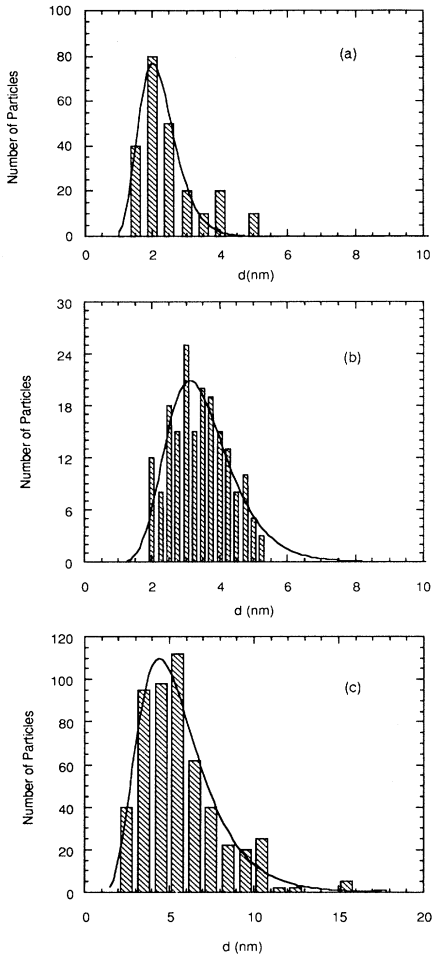

FIG. 12. Dependence of size distribution on the double-annealing procedure carried out at (a) 300 °C and (b)–(d) 600 °C. Each annealing time was 30 min.

G. Size dependence of photoluminescence

In nc-Ge the effective masses for electrons and holes are very light; therefore, if the PL energy obeys the simple quantum confinement in QD's, the PL energy should shift significantly within a narrow-size region. When the size changes from 4 to 8 nm, the predicted PL energy should shift from 2.6 to 1.2 eV. This energy change ranges over the visible wavelength region as discussed later. This PL behavior shows that we need to control the average size and dispersion in such a small-size region. Using the double-annealing procedure, the size inhomogeneity of nc-Ge can be controlled precisely.

Figures 13(a)–13(d) show PL spectra at room temperature (300 K) for (a) $d_g=2.1$ nm, $\sigma=1.28$ nm, (b) $d_g=3.3$ nm, $\sigma=1.35$ nm, (c) $d_g=4.8$ nm, $\sigma=1.6$ nm, and (d) $d_g=6.0$ nm, $\sigma=1.8$ nm. As the average size increases, both a clear redshift of the PL peak from 2.3 to 2.13 eV (as shown by the arrows in Fig. 13) and inhomogeneous broadening of the PL spectrum are observed, and simultaneously the intensity changes significantly; for example,

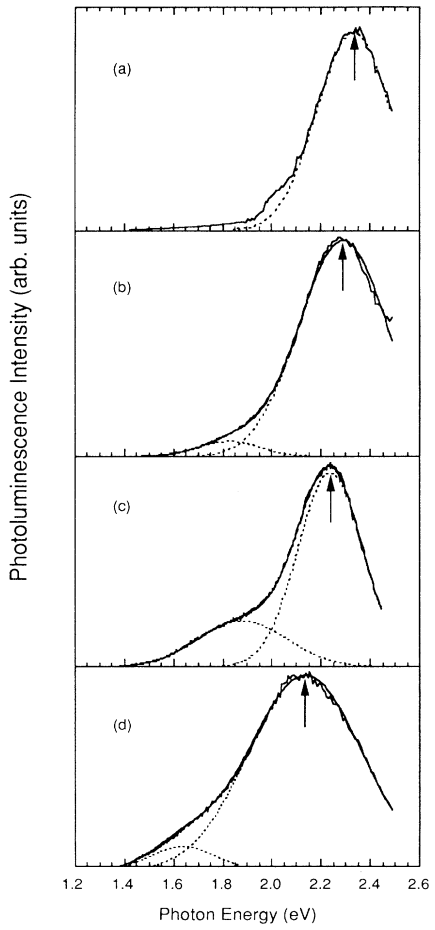

FIG. 13. Room-temperature photoluminescence spectra obtained after the double annealing. The PL was excited by a 488-nm Ar-ion laser.

the intensity of (d) is one-tenth that of (a) (size range between 2.1 and 6.0 nm), on the other hand, the peak energy can shift only in a smaller range between 2.1 and 2.4 eV than that predicted by a three-dimensional quantum-confinement model.

Figure 14 shows the PL spectra for the as-deposited sample, which are excited by an Ar-ion laser (488 nm) or a He-Cd laser (325 nm). Under the excitation of the Ar-ion laser no pronounced or even very weak PL [one-fifth of the spectrum (a)] is observed at both RT and liquid-nitrogen temperature (77 K). Under the excitation of the He-Cd laser clear PL is observed at 3.1 eV, which can be seen to be blue. The peak intensity of the PL spectrum (a) is about one-hundredth of that shown in Fig. 13(a). The PL peak intensity at 3.1 eV increases as temperature decreases from room temperature to 77 K. The PL spectra (a) and (b) show temperature dependence of the intensity that is the same as that reported by Skuja[19] in Ge-doped glassy SiO_2. In Sec. IV, related luminescent defects (Ge E' centers) are discussed. As mentioned about the precipitation of very small size ($d \leq 3$ nm) nc-Ge as shown in Fig. 11, when the sample is annealed at such a

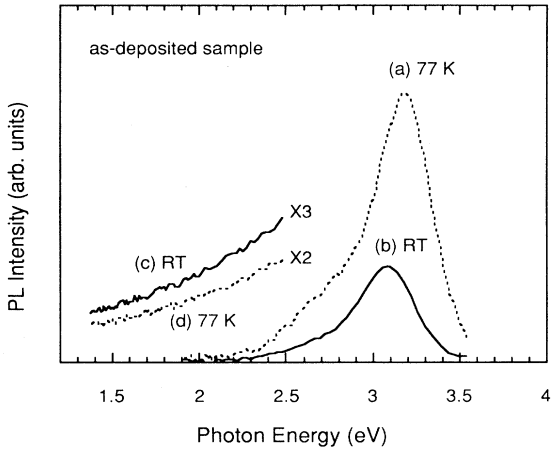

FIG. 14. Photoluminescence spectra obtained in the as-deposited sample at RT and 77 K. The PL spectra (a) and (b) were excited by a 325-nm He-Cd laser, and the weak spectra (c) and (d) were done by a 488-nm Ar-ion laser.

low temperature T_n the size cannot increase, but the number of nc-Ge increases with increasing annealing time. Figure 15 shows the increase of the PL intensity as a function of annealing time. The PL intensity increases and the peak energy is located at the same energy of 2.3 eV. This intensity increase can be related to the increase of the number of nc-Ge that can be calculated from the average nucleation rate I ($=4.4\times10^{14}$ $cm^{-3}s^{-1}$). This shows that the actual nucleation rate is decreased by lowering the driving force $\Delta\mu$ in Eq. (2b). From the dependence of the PL intensity and independence of the PL energy on the density of nc-Ge with almost the same size, we can confirm a strong correlation between the PL intensity and the increase of the number of nc-Ge. This result is consistent with the quantum confinement as discussed later.

Figure 16 shows photographs for PL exhibiting colors from green to yellowish orange that correspond to the PL

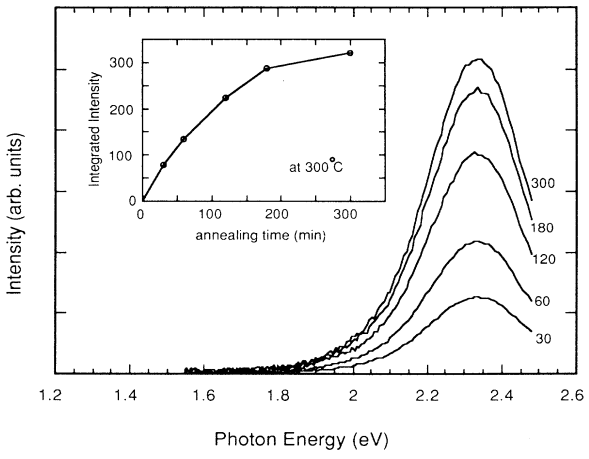

FIG. 15. Integrated intensity of PL spectra of the sample annealed at 300 °C as a function of the annealing time.

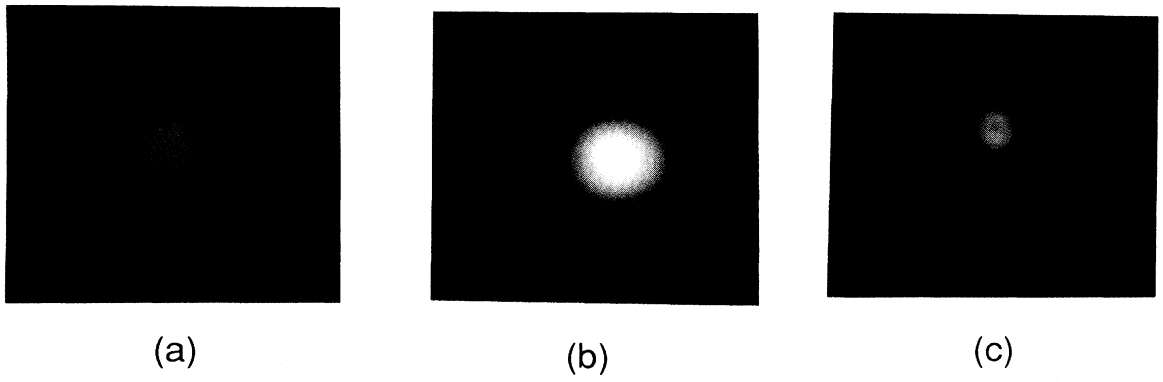

FIG. 16. Photographs of the PL emission for (a) green, (b) yellow, and (c) yellowish orange under excitation of a 488-nm Ar-ion laser.

spectra (a), (b), and (d) in Fig. 13. These photographs were taken through the cut filter of a 488-nm excitation laser. We can see these luminescences with the naked eye under 1-mW Ar-ion laser excitation at room temperature. After preparation of samples with an average size from 2 to 14 nm by the double-isothermal annealing procedure, the PL peak energy and the intensity were examined by the same method.

Figure 17 shows the size dependence of PL energy and the integrated intensity normalized by the density of nc-Ge. The PL peak energy shows a blueshift only for sizes between 2 and 5 nm. With sizes larger than 5 nm the PL peak energy shows a constant energy at 2.0–2.1 eV. The integrated intensity shows significant change in the same size range. These behaviors are far from those predicted by the simple quantum-confinement model given by Eq. (6). These results mean that there is a critical size showing the quantum-size effect and this critical size is roughly smaller than 5 nm.

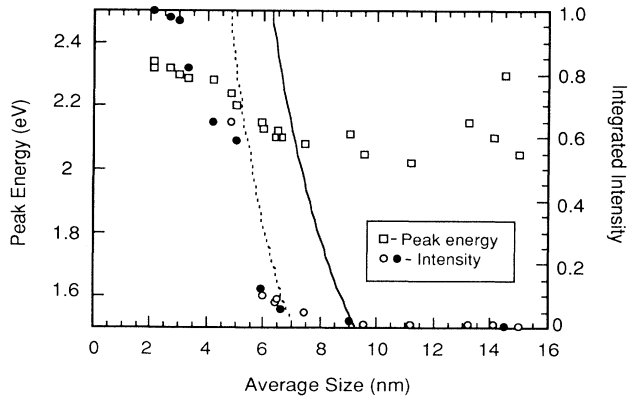

FIG. 17. Size dependence of PL peak energy and the integrated intensity normalized by the nc-Ge density. The solid and dotted curves correspond to the size dependence of the PL energies for reduced masses $\mu=0.021m_0$ and $0.036m_0$, respectively. The size denoted by circles was measured by Raman spectrometry, and that of shaded circles was done by HR-TEM.

H. Excitation bands

To measure the excitation bands for the visible PL observed above, PL excitation spectra were measured at room temperature. Figure 18 shows the PL spectrum for $d_g=5.2$ nm and $\sigma=1.5$ nm and the PLE spectra obtained at the measurement energies from (a) to (d) of the PL spectrum. The PLE spectrum depends on the measurement energy of the PL spectrum and it shows a peak

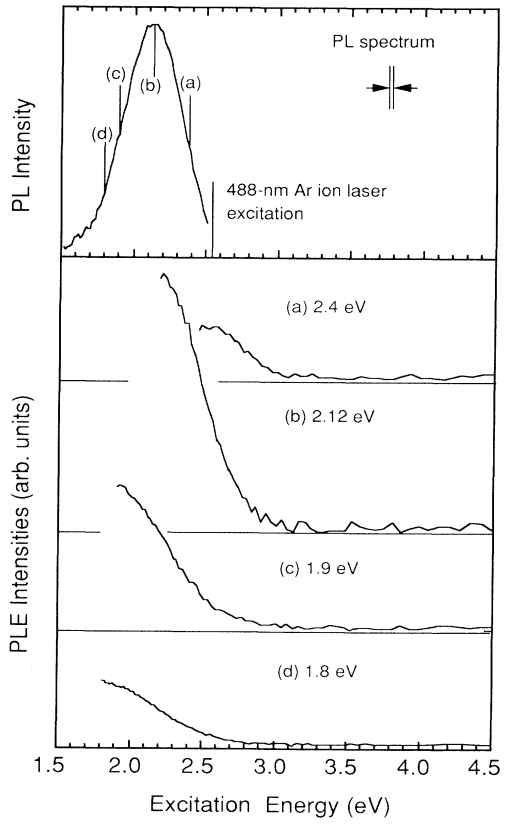

FIG. 18. Photoluminescence excitation (PLE) spectra at measurement energies (a)–(d) of the PL spectrum.

close to that of the measurement energy and with a narrow excitation-bandwidth. The Stokes shifts are observed to be smaller than 0.1 eV. The excitation band has 0.2–0.3-eV bandwidth. Skuja[19] reported an excitation band at 4.3 eV associated with Ge E' defects. But for the present study, no excitation bands can be observed at the energy larger than 3 eV. The PLE measurement results mean that there are many different and inhomogeneous excitation bands for the PL, which are associated with the size inhomogeneity of nc-Ge and there are no contributions of excitation bands coming from luminescent defects.

IV. DISCUSSION

A. Quantum confinement

The observation results reveal that the visible PL is strongly correlated to the presence of nc-Ge in the sample. Then we attempted to interpret the quantitative properties by a simple quantum-confinement model. If Wannier excitons are confined in an infinite spherical-symmetry potential (QD's), the exciton Bohr radius a_B can be regarded as the critical size that distinguishes between two different situations of quantum confinement.[20] The exciton Bohr radius is given by $a_B=\kappa\hbar^2/\mu_{e\text{-}h}e^2$, where $\hbar$ is the Planck constant, κ is the static dielectric constant (Ge: $\kappa=16.3$), $\mu_{e\text{-}h}$ is the reduced mass for excitons given by $1/\mu_{e\text{-}h}=1/m_e^*+1/m_h^*$. m_e^* and m_h^* are effective masses for electrons and holes, respectively, and e is an electron charge. In the case of Ge, we get the average effective mass of electrons at L, $m_r^*=0.04m_0$, using $1/m_r^*=(1/m_l+2/m_t)$, and $m_t=0.082m_0$, and $m_l=1.58m_0$, which are the transversal and longitudinal masses, respectively (m_0: electron masses). The reduced masses $\mu_{e\text{-lh}}=0.021m_0$ and $\mu_{e\text{-hh}}=0.036m_0$ are obtained using $m_r^*=0.04m_0$ and the effective masses for heavy holes and light ones, $m_{\text{lh}}^*=0.043m_0$ and $m_{\text{hh}}^*=0.32m_0$. Therefore, $a_B=22.6$–38.8 nm and the exciton binding energy $E_{\text{Ry}}^*=\mu e^4/2\hbar^2\kappa^2=1.1$–$1.8$ meV can be obtained. The ratio $\rho=R/a_B$ is very useful to evaluate the physical situation of the excitons confined in the QD's. In the actual size range observed in the HR-TEM images, ρ is much smaller than 1. In this case using the zeroth-order approximation the asymptotic wave function

$$\Psi(r_e,r_h,r_{eh})=j_0[\pi r_e/R]j_0[\pi r_h/R](1-Cr_{eh}) \tag{5}$$

can be employed, where $j_0(x)$ is the zeroth-order spherical Bessel function. C is the constant of $0.498.../a_B$. For $\rho\leq 1$, we can consider that electrons and holes are confined independently in the QD's in radius R, and the energy can be given by

$$E_{nl}=E_g+\hbar^2/2\mu_{e\text{-}h}(\alpha_{nl}/R)^2 - 1.786e^2/\kappa R - 0.248E_{\text{Ry}}^*\ , \tag{6}$$

where E_g is a band-gap energy and α_{nl} is the eigenvalue of the zeroth-order spherical Bessel function ($\alpha_{10}=\pi$, $\alpha_{11}=4.4934$, $\alpha_{12}=5.7635$, $\alpha_{20}=6.2832,...$).[20] The second term gives kinetic energies of electrons and holes, the third one is a Coulomb interaction energy, and the fourth one is the remnant of the exciton effect. The lowest energy E_{10} can be obtained using Eq. (6) and $E_g=0.66$ eV at 300 K, in nc-Ge of $R=2$–4 nm, $E_{10}=1.3$–2.67 eV. This lowest energy range agrees semiquantitatively with the observed PL energy in Fig. 13. The small discrepancy between the calculation and experimental energies may be due to overestimation of the effective masses of electrons and holes.

This simplest calculation of an independent confinement of electrons and holes in nanocrystallite Ge ignores the indirect band gap of Ge ($\Gamma'_{25}-L_2$). A detailed discussion on the possibility of a radiative process between indirect band gaps requires more accurate calculations. Takagahara and Takeda[21] calculated the confinement energy and radiative decay rate for the Wannier exciton energy in Si and Ge QD's as a function of the dot radius, taking into account optical transitions between indirect band gaps of Si and Ge. According to their calculation, in Ge QD's the exciton energy changes significantly in the dot radius less than 2.5 nm because of a lighter electron mass. In their calculation we can also see the same size dependence of exciton energy as that observed in this study. The most noticeable change in the radiative rate takes place in the same radius range. They showed the possibility of luminescence originating from excitons confined in Si and Ge QD's. They also pointed out the presence of nonradiative relaxation channels of excitons that can modify exponential decay to a nonexponential one. The decay constant of the PL has been measured as ~ 1 ns and the internal emitting efficiency η has been measured as $\sim 0.5\%$,[4]

$$\eta=1/[1+(\tau_r/\tau_n)]\ , \tag{7}$$

where τ_n and τ_r are the lifetimes for a nonradiative recombination and a radiative one. Using $\tau_r=10^{-9}$ s and $\eta=5\times10^{-3}$, we get τ_n on the order of 10^{-11} s. Such a nonradiative relaxation procedure might take place at surface dangling bonds of nc-Ge or the interface between nc-Ge and the SiO_2 matrix. The presence of dangling bonds at the nc-Ge surface affects the radiative efficiency, and determines the actual situation whether we can observe the luminescence or not. From this viewpoint, the surface oxides of nanocrystallites are important for enhancement of radiative efficiency. If a termination between Ge and O at the nc-Ge surface can be formed, this Ge-O bonding gives a barrier potential larger than 4 eV. In this case, nonradiative channels can be inhibited, so that we can get enough radiative efficiency to observe the visible luminescence with the naked eye. By taking into account such a fast nonradiative relaxation, the effective radius for radiative relaxation of excitons, which depends on the radius, can be estimated to be ~ 2 nm. This critical radius shows a good agreement with that observed in Fig. 14 showing the PL intensity and the energy as a function of the size.

B. Luminescent Ge E' centers in silica glasses

The Ge-doped glassy SiO_2 matrix used as the starting material is known to exhibit PL coming from luminescent

centers (E' centers) which originate from defects formed in SiO_2 glassy networks. For example, Skuja[19] reported that Ge-doped glass (10 mol % GeO_2-SiO_2) showed PL at 3.1 eV at 293 K with a long decay constant of ~ 113 μs under Xe lamp or N_2 laser excitation, and the excitation band for the PL was observed to extend above 4.6–5.0 eV. This excitation band due to Ge E' centers has been related to second harmonic generation and self-organization of Bragg lattice reflectors (BLR) in optical fibers consisting of the 10 mol % GeO_2-SiO_2 glass. In the BLR formation, a two-photon absorption process due to the Ge E' center (~ 5 eV) was observed to take place in the excitation of the Ar-ion laser (488 nm, 2.5 eV). Kohketsu *et al.*[22] and Awazu, Muta, and Kawazoe[23] reported that in Ge-doped silica glasses sintered under a hydrogen atmosphere, red PL with peaks at 650–680 nm could be observed with two-photon excitation by an Ar-ion laser of 2.5 eV, and that the red-band PL was due to two-photon excitation ($E = 5.14$ eV) between the Ge lone-pair centers of $X'\Sigma^+$ and $A'\Pi$ and radiative recombination ($E = 1.83$ eV) between the germyl radicals. Both groups[22,23] also reported that a weak light source, for example, a monochromatized Xe lamp, could not excite any PL and originally Ge E' centers are related to hydrogen annealing. They observed at typical Raman peak at 1060 cm^{-1} due to Si-O-Si stretching in the PL spectra. When we compare the PL spectra measured in this paper with those of Refs. 22 and 23, the apparent properties of the PL spectra seem to be similar. However, the same PL spectra as those excited by an Ar-ion laser can also be excited by the weak Xe lamp and in those PL spectra no Raman peaks are observed because of the much stronger intensities of the PL peaks. Furthermore, there is a big difference also in the excitation bands measured in the PLE spectra, and the decay constants (~ 0.9 ns)[4] are smaller than the decay constant (~ 100 μs) due to Ge E' centers reported in Ref. 19. The Ge-related defects (Ge E' centers) in silica glasses are not the origin of the PL observed in this paper because of the big differences in those PL properties.

C. Phase transition of nanocrystallites

Veprek, Iqbal, and Sarott[24] suggested there was instability of the diamond lattice of Si when the film thickness decreased significantly. They reported that a structural transition from the diamond structure to the amorphous phase took place below the thickness of about 3 nm. In a thermodynamical consideration, the large driving force for this structural transition comes from the large difference between surface energy and internal energy of the diamond structure when the size decreases. The critical size may depend on the energy of the dominant surface, in Si and Ge, the {111} planes. From a thermodynamical-energy balance, the critical size can be estimated to be about 2 nm, which shows good agreement with experiments. Also in the case of nanocrystallite Ge the same instability of the diamond lattice can be considered to take place. In Fig. 10(a) the lattice spacing changes from the usual one of {111} to another. This change probably comes from lattice instability or a structural transition from the diamond to another structure; this has already been reported by Saito[14] and Hayashi *et al.*[15] So we tried to observe the structure and the electron diffraction (ED) of nc-Ge smaller than 4 nm in size with HR-TEM. We confirm that for about ~ 4-nm size the observed lattice fringes and the ED pattern agree with those for the diamond-structure Ge. Furthermore, to examine the actual electronic structure, electron-energy-loss spectrum (EELS) measurements using a nanometer-sized electron beam were carried out. It has been observed that plasmon-loss peaks (located at 17.8 and 16.5 eV in 2 and 10 nm) showed a clear size dependence.[25] This increase of plasmon-loss energy could be explained from a quantum-size effect of the band gap that affected the plasmon energy through the oscillator strength as reported in EELS measurements of Si clusters.[26] The EELS measurements do not support the significant change in the electronic structure caused by the structural transition, and we can conclude that nc-Ge of ~ 4 nm in size has a diamond structure or a very close structure to it. However, structural transitions in very-small-size crystallites or clusters have to be analyzed more as one of the candidates for the origin of visible PL.

V. CONCLUSIONS

We studied precipitation behaviors and size inhomogeneity and determined that they were the product not of the usual simple diffusion procedure of Ge, but of a complicated procedure including reduction of Ge oxides by Si. Using a double-annealing procedure carried out at two characteristic temperatures, we could control the size inhomogeneity in very-small-size steps. The properties of photoluminescence observed in a visible wavelength range showed a strong correlation to the change in the size. These PL properties seemed to be more consistent with the properties predicted by a quantum-confinement model in Ge QD's than those predicted by other models. The discrepancy with the quantum-confinement model may come from the presence of fast nonradiative relaxation channels in nc-Ge, taking place at the surface.

ACKNOWLEDGMENTS

The author would like to acknowledge Dr. N. Kinjo and Dr. T. Minemura for encouragement of this study. He also thanks N. Tsukamoto, M. Nagai, and K. Kato for their collaboration in PL measurements and sample preparation, and Dr. F. Leblanc for his valuable suggestions on interference effects of PL spectra.

[1] L. T. Canham, Appl. Phys. Lett. **57**, 1046 (1990).

[2] See, for example, *Light Emission from Silicon*, edited by S. Iyer, R. Collins, and L. Canham, MRS Symposia Proceedings No. 256 (Materials Research Society, Pittsburgh, 1992).

[3] Y. Maeda, N. Tsukamoto, Y. Yazawa, Y. Kanemitsu, and Y. Masumoto, Appl. Phys. Lett. **59**, 3168 (1991); Y. Maeda, H. Uto, Y. Kanemitsu, and Y. Masumoto, *Extended Abstracts of SSDM'92* (The Japan Society of Applied Physics, Tsukuba,

1992), p. 379.
[4]Y. Kanemitsu, H. Uto, Y. Masumoto, and Y. Maeda, Appl. Phys. Lett. **61**, 2187 (1992).
[5]R. Venkatasubramanian, D. P. Malta, M. L. Timmons, and J. A. Hutchby, Appl. Phys. Lett. **59**, 1603 (1991).
[6]D. C. Paine, C. Caragianis, T. Y. Kim, and Y. Shigesato, Appl. Phys. Lett. **62**, 2842 (1993).
[7]D. C. Paine, C. Caragianis, and Y. Shigesato, Appl. Phys. Lett. **60**, 2886 (1992).
[8]M. Fujii, S. Hayashi, and K. Yamamoto, Jpn. J. Appl. Phys. **30**, 687 (1991).
[9]R. Hayashi, M. Yamamoto, K. Tsunetomo, K. Kohno, Y. Osaka, and H. Nasu, Jpn. J. Appl. Phys. **29**, 756 (1990).
[10]I. Barin and O. Knacke, *Thermodynamical Properties of Inorganic Substances* (Springer, Berlin, 1973).
[11]This thermodynamical calculation assumed that all the elements such as Ge, Si, and O were pure, at the standard state, and their activities were $a=1$. However, these assumptions are not correct because small amounts of Si and Ge dissolve in the SiO_2 matrix as a solid solution.
[12]G. A. Wolff and J. G. Gualtieri, Am. Mineral. **47**, 562 (1962).
[13]G. Wulff, Z. Kristallogr. **34**, 449 (1901).
[14]Y. Saito, J. Cryst. Growth **47**, 61 (1979).
[15]S. Hayashi, H. Wakayama, T. Okada, S. S. Kim, and K. Yamamoto, J. Phys. Soc. Jpn. **56**, 243 (1987).
[16]A. I. Ekimov and A. A. Onushchenko, Fiz. Tekh. Poluprovodn. **16**, 1215 (1982) [Sov. Phys. Semicond. **16**, 775 (1982)].
[17]I. M. Lifshitz and V. V. Slyozov, Zh. Eksp. Teor. Fiz. **35**, 479 (1958) [Sov. Phys. JETP **35**, 331 (1959)].
[18]B. G. Potter and J. H. Simmons, Phys. Rev. B **37**, 10 838 (1988).
[19]L. Skuja, J. Non-Cryst. Solids **149**, 77 (1992).
[20]Y. Kayamuma, Phys. Rev. B **38**, 9797 (1988).
[21]T. Takagahara and K. Takeda, Phys. Rev. B **46**, 15 578 (1992).
[22]M. Kohketsu, K. Awazu, H. Kawazoe, and M. Yamane, Jpn. J. Appl. Phys. **28**, 622 (1989).
[23]K. Awazu, K. Muta, and H. Kawazoe, J. Appl. Phys. **74**, 121 (1993).
[24]S. Veprek, Z. Iqbal, and E. A. Sarott, Philos. Mag. B **45**, 137 (1982).
[25]Y. Maeda (unpublished).
[26]M. Mitome, Y. Yamazaki, H. Takagi, and T. Nakagiri, J. Appl. Phys. **72**, 812 (1992).

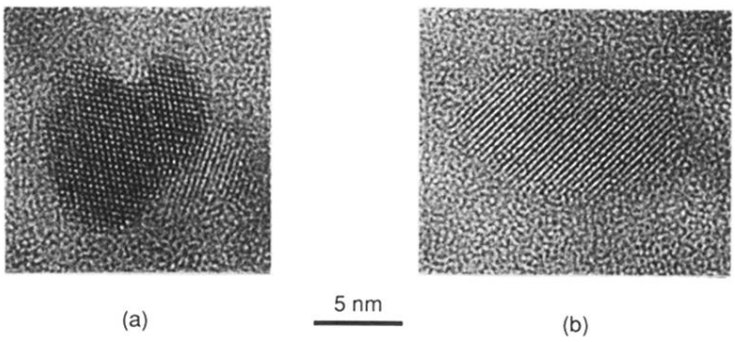

FIG. 10. HR-TEM images of nc-Ge in an aggregation process during annealing.

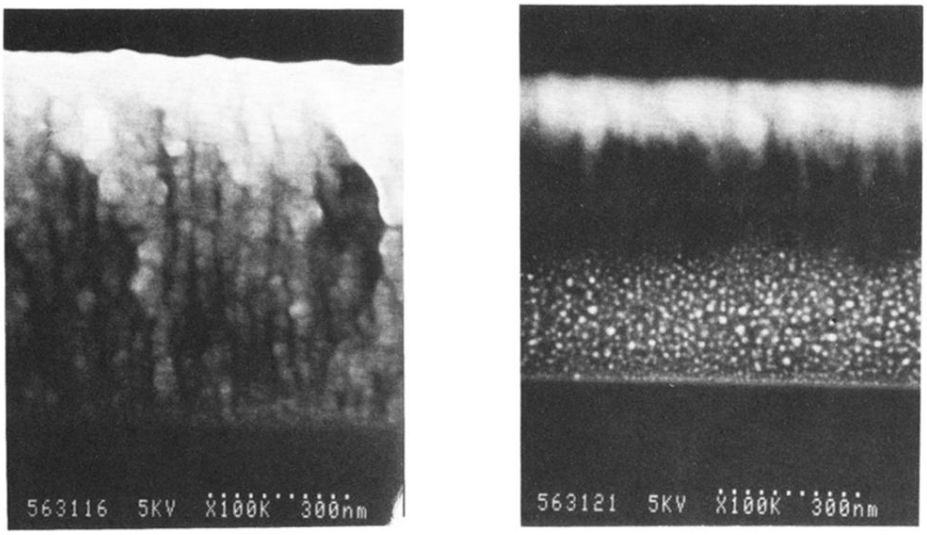

FIG. 1. Cross-sectional SEM images for (a) the as-deposited sample and (b) the annealed sample (800 °C, 30 min).

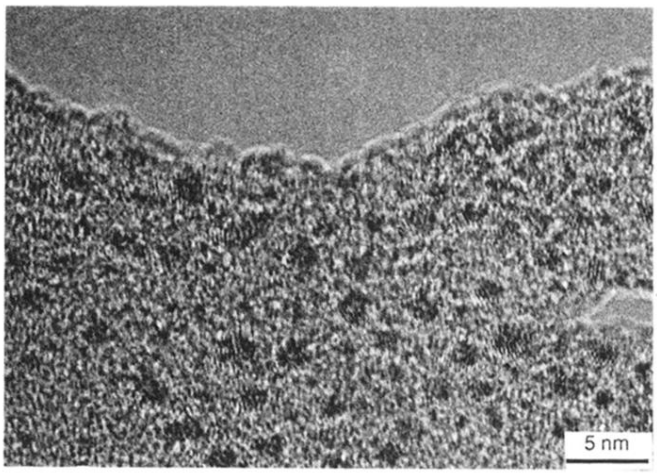

FIG. 11. HR-TEM image of very small nc-Ge close to the critical size for nucleation.

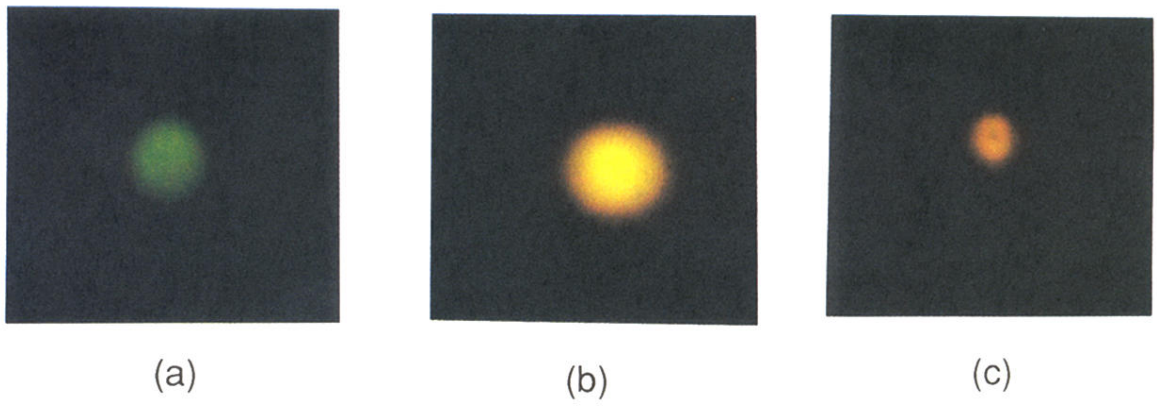

FIG. 16. Photographs of the PL emission for (a) green, (b) yellow, and (c) yellowish orange under excitation of a 488-nm Ar-ion laser.

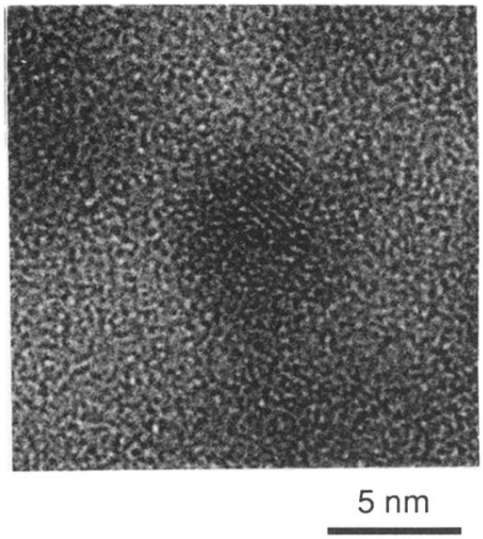

FIG. 3. HR-TEM image of 2–3-nm-sized nc-Ge with diffuse lattice fringes. The annealing was carried out at 300 °C for 30 min.

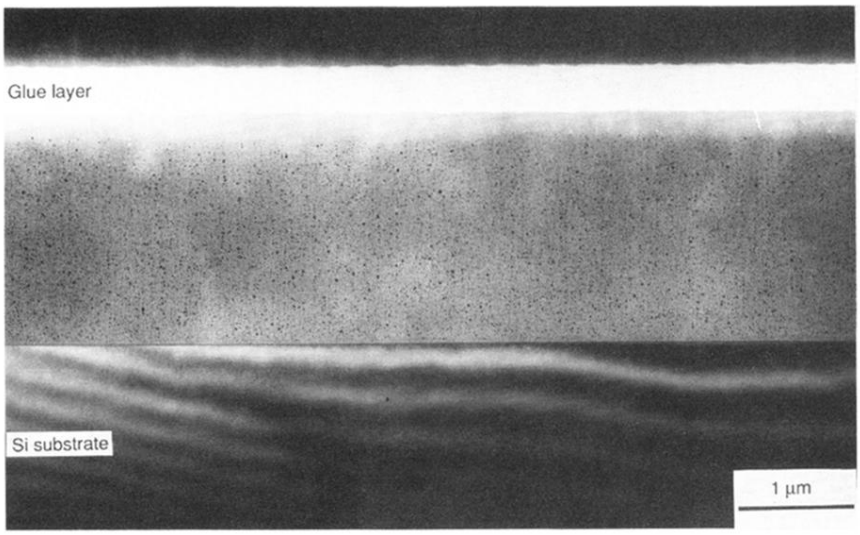

FIG. 5. Cross section of the matrix exhibiting a large number of nc-Ge in a precipitation layer.

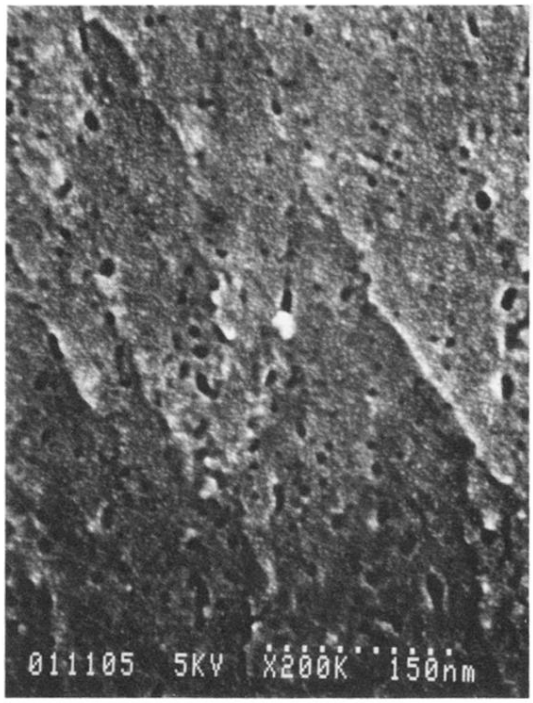

FIG. 7. SEM image of the cross-sectional structure of the sample exhibiting a large number of pores. The surface was coated with a thin Pt film.

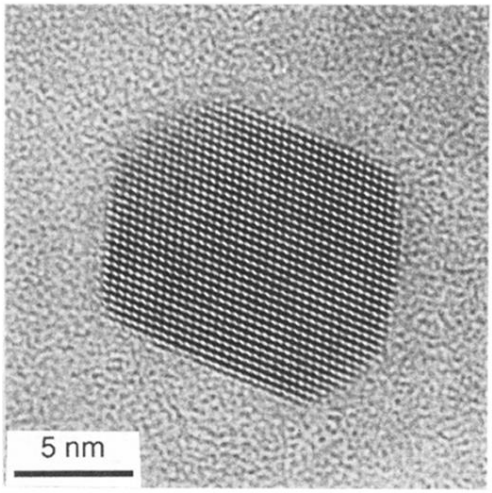

FIG. 8. HR-TEM image of well-grown nc-Ge with the actual size of 15 nm.

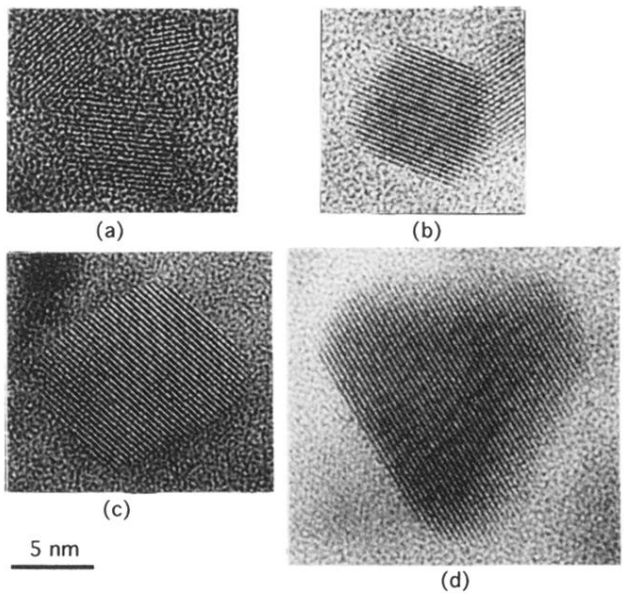

FIG. 9. Size dependence of crystallite morphologies.